Spectroscopic Determination of Dynamic Plasma Gradients in Implosion Cores

I. Golovkin,[1] R. Mancini,[1,*] S. Louis,[2] Y. Ochi,[3] K. Fujita,[3] H. Nishimura,[3] H. Shirga,[3] N. Miyanaga,[3] H. Azechi,[3] R. Butzbach,[4] I. Uschmann,[4] E. Förster,[4] J. Delettrez,[5] J. Koch,[6] R. W. Lee,[6] and L. Klein[7]

[1]*Department of Physics, University of Nevada, Reno, Nevada 89557*
[2]*Department of Computer Science, University of Nevada, Reno, Nevada 89557*
[3]*Institute of Laser Engineering, Osaka University, Osaka, Japan*
[4]*Institute of Optics and Quantum Electronics, Jena University, Jena, Germany*
[5]*Laboratory for Laser Energetics, University of Rochester, Rochester, New York 14623*
[6]*Lawrence Livermore National Laboratory, University of California, Livermore, California 94550*
[7]*Department of Physics and Astronomy, Howard University, Washington, D.C. 20059*

(Received 12 June 2001; published 10 January 2002)

The time-dependent gradient structure of a laser-compressed, high-energy-density plasma has been determined using a method based on the simultaneous analysis of time-resolved x-ray monochromatic images and x-ray line spectra from Ar-doped D_2 implosion cores. The analysis self-consistently determines the temperature and density gradients that yield the best fits to the spatial-emissivity profiles and spectral line shapes. This measurement is important for understanding the spectra formation and plasma dynamics associated with the implosion process. In addition, since the results are independent of hydrodynamic simulations, they are also important for comparison with fluid-dynamic models.

DOI: 10.1103/PhysRevLett.88.045002 PACS numbers: 52.57.Fg, 32.30.Rj, 52.50.Lp, 52.70.La

In this Letter, a measurement of the dynamic gradients in the core of a stable implosion is presented. Previous implosion studies have failed to address the gradient problem, even though hydrodynamic simulations predicted significant gradients in these plasma conditions. The work that we describe is a unique attempt to address this problem through the analysis of time-resolved x-ray images and line spectra of the implosion process. As implosion dynamics are an essential component of inertial confinement fusion and important to applications involving spectroscopy diagnostics, the present quantitative measurement of the hydrodynamic behavior of a stable implosion is a significant step in developing a predictive capability. The evolution of the plasma gradients is also of basic relevance to atomic physics studies of level population kinetics, electron thermal conduction, radiation energy coupling and transfer, and spectral line formation.

Although spatially resolved measurements of plasma conditions at these high-energy densities have not been carried out in the past, the study of the average properties of laser compressed plasmas has progressed from experimental measurements of peak electron densities in the compressed core [1], to the determination of spatially averaged, but temporally resolved, electron temperatures, $\langle T_e(t)\rangle$, and densities, $\langle N_e(t)\rangle$ [2,3]. The temporally resolved data augmented by a comparison with hydrodynamic simulations provided significant information on the evolution of the implosion [4]. Parallel to these experimental developments, the iterative comparison of the spectral data with a theoretical computation of the spectrum emitted at an effective temperature and density [5] has become a standard tool to extract the $\langle T_e(t)\rangle$ and the $\langle N_e(t)\rangle$ for a diagnostic study of the emitting medium [6]. Hence, such studies are also an important source of information on the accuracy of theoretical line shape computations [7]. Nevertheless, although the experimental results cited above were a substantial improvement over earlier work, one finds that the investigation of certain fundamental effects in the spectral profile, such as ion dynamics and plasma line shifts, require a better characterization of the plasma source because of the possibility that spatial gradients affect the analysis [8].

The core gradient measurement in the stable, reproducible implosion conditions presented here also provides an excellent source of data for an assessment of radiation-hydrodynamic simulation codes, since comparison of the measured gradient with computations of the implosion conditions gives an important reference point for modeling of the dynamics involved. The analysis can therefore be considered to be the first step in a program to provide a simulation free benchmark for both spectral syntheses and hydrodynamic simulations. In stronger implosions or unstable plasma conditions, other nonspectroscopic diagnostic techniques are used to investigate the hydrodynamic models [9].

The gradient measurement is based on temporally and spatially resolved spectral data recorded in a series of directly driven microsphere implosion experiments performed at the Osaka University GEKKO XII laser system. The array of diagnostics instrumentation included a monochromatic x-ray framing camera, essential for the spatial resolution of the plasma [10]. The x-ray monochromatic images were used to obtain, for the first time in an implosion experiment, spatially and temporally resolved data on the collapsing core. In addition, time-resolved, but spatially averaged, streak spectrograph spectral data for the usual spatially averaged diagnostic were recorded. We note that the additional image information was required

since core plasma gradients cannot be unambiguously determined based solely on the analysis of space-integrated x-ray spectra. The drive consisted of a 12 beam, 2.55 kJ Nd glass laser operating at 526 nm. Random phase plates were used to smooth individual beams. The laser pulse was composed of a 0.2 ns prepulse followed by a 1.6 ns square pulse with rise time of 0.05 ns. The prepulse is important for the stabilization of the implosion [11]. Targets were plastic shells, 500 μm in diameter, with 8 μm wall thickness, filled with 30 atm of D_2 and doped with 0.075 atm of Ar (for diagnostic purposes). The implosion is diagnosed by recording both the compressed core image and the Ar spectrum. In particular, time-resolved x-ray monochromatic images and simultaneous spatially integrated x-ray spectra of the Ar XVII $1s^2\ ^1S$-$1s3p\ ^1P$ transition (Heβ) were recorded. For the spatial information, a two-dimensional x-ray monochromatic framing camera imaging the central 19 eV of the Heβ line emitted by the Ar in the core was employed. This x-ray imager monitors the implosion symmetry and provides up to five frames with $\Delta t = 40$ ps duration, 50 ps interframe time, and 10 μm spatial resolution [10]. The x-ray spectrometer consisted of a flat RbAP (100) crystal coupled to an x-ray streak camera with 10 ps time resolution and resolving power, $\lambda/\Delta\lambda$, of 600. It is important that the entire core of the implosion is in the field of view of the spectrograph so that a spatial average over the imploded core radius is recorded for the determination of both $\langle T_e(t)\rangle$ and $\langle N_e(t)\rangle$. As an example of both types of data, the second frame, Δt_2, recorded by the imager in the interval 342–382 ps, and the x-ray streak spectrograph, with the same time interval marked, are presented in Fig. 1.

As has become standard for diagnostic purposes in implosion investigations, argon is mixed into the lower-Z gas-filled microsphere at concentrations low enough to ensure that the transition of interest is optically thin and easily observable [2,3]. A detailed analysis of the line profile of the Ar He_β transition at 3680 eV and its associated Ar Li-like satellite structure is used to derive the spatially averaged electron temperature and density. To ensure that optical depth effects do not compromise the line profile, a detailed radiation transport calculation is performed [12]. The uniform-plasma-model analysis of the time-resolved spectral data, integrated over the 40 ps time interval corresponding to the second imager frame (see Fig. 1), yields the spatially averaged values, $\langle T_e\rangle = 620$ eV and $\langle N_e\rangle = 3 \times 10^{23}$ cm^{-3}. The corresponding synthetic spectra fit to the data is shown in Fig. 2.

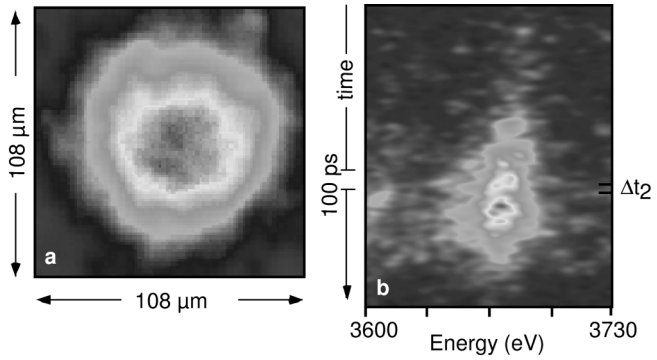

FIG. 1. (a) Ar Heβ monochromatic image frame, recorded in the interval $\Delta t_2 = 342$–382 ps; (b) time-resolved Ar Heβ spectra with the time interval Δt_2 marked on the time axis.

In order to extract the temperature and density gradients from the spectral data, the spatially averaged plasma parameters deduced from the spectral line shape measurement must be associated with the simultaneously recorded monochromatic image information. The observation that these average values are emissivity averages [8] is key to the untangling of the local temperature and density values from this functional relationship. That is, it has been shown in a previous study [12] that the $\langle T_e(t)\rangle$ and $\langle N_e(t)\rangle$ found from the line shape data are best fit with average plasma parameters that are calculated from the values, $T_e(r,t)$ and $N_e(r,t)$, with the monochromatic emissivity $\varepsilon_{\nu_0}(r,t)$ as a weighting function.

The image data containing the spatial and temporal information required for the determination of the monochromatic emissivity, $\varepsilon_{\nu_0}(r,t)$, must be mapped onto the radial coordinate system by using a spherically symmetric Abel inversion of each image [13]. Figure 3 shows the $\varepsilon_{\nu_0}(r,t)$ obtained from the Abel inversion of the monochromatic image from the time interval, Δt_2, of Fig. 1a. A major source of error in the gradient determination is the deviation from spherical symmetry observed in the image of the implosion. This asymmetry can be seen, for example, in the image of Fig. 1. In Fig. 3, we show a measure of the effect of this asymmetry on the Abel inverted emissivity, $\varepsilon_{\nu_0}(r,t)$, by plotting the standard deviation from radial symmetry derived from reading the image data in Fig. 1

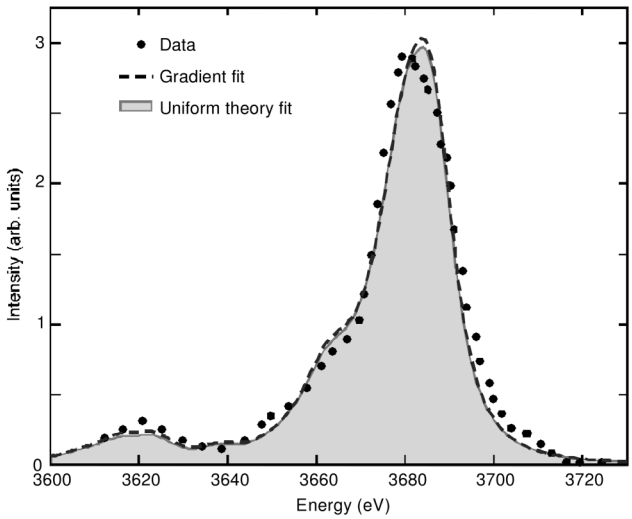

FIG. 2. Synthetic spectra fits to the Ar Heβ spectrum, time integrated over the same interval as Δt_2. The circles represent the data; the dashed line is the nonuniform plasma model fit using self-consistent gradients, while the gray profile is the uniform plasma model fit with $\langle T_e\rangle = 620$ eV and $\langle N_e\rangle = 3.0 \times 10^{23}$ cm^{-3}.

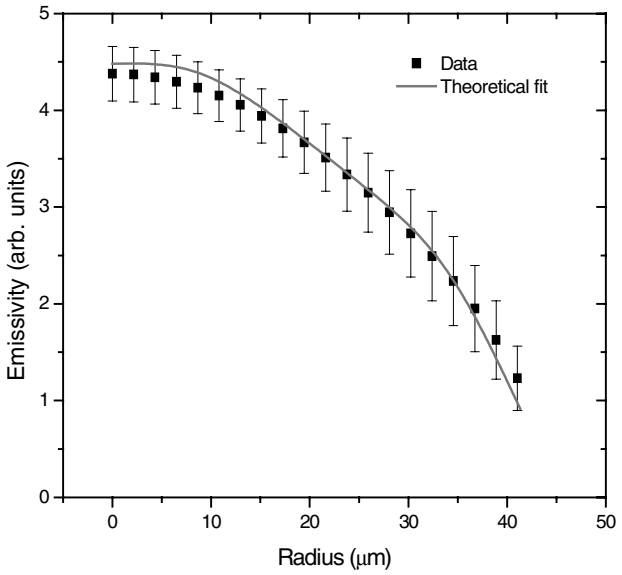

FIG. 3. The Ar Heβ emissivity spatial profile for frame Δt_2. The squares with error bars represent the data, and the solid line is the emissivity fit derived self-consistently with the T_e and N_e gradients. The error bar indicates the variation in the emissivity resulting from the variation in the Abel inversion due to the deviation from spherical symmetry.

along eight different (uniformly spaced in angle) radial directions.

We now describe the self-consistent iterative procedure that, at a given time, seeks the set of temperature and density gradients, $T_e(r,t)$ and $N_e(r,t)$, that yield the best fits to the spatially resolved monochromatic emissivity and the spatially integrated He$_\beta$ spectral line profile, consistent with the results obtained from the analysis of the spectrum using a uniform plasma model approximation. The experimental spectrum of Fig. 2 and the emissivity of Fig. 3 are fit to the synthetic spectrum and emissivity calculated with the spectral model of Ref. [12], with input $T_e(r,t)$ and $N_e(r,t)$ determined by the iterative search procedure. To efficiently implement the self-consistent iterative search procedure, a multicriteria search and optimization genetic algorithm technique for inverting spatially and temporally resolved data has been developed. Genetic algorithms (GA) start from a randomly selected initial population, are very robust, and are not likely to get caught in local minima. They are search and optimization algorithms based on the mechanics of natural selection [14]. The GA used here was first tested in the analysis of space-integrated time-resolved x-ray spectral data; this is a single criterion problem where the GA searches a two-dimensional parameter space (i.e., T_e and N_e) for the (T_e, N_e) set that yields the best fit to the data based on a least-square minimization [15]. This algorithm-driven technique was extended to the gradient analysis, which is a two-criteria problem where both spectrum and emissivity have to be simultaneously fit. The multicriteria aspect was handled with a niched-Pareto optimality technique that works with a distribution of solutions obtained by the GA (i.e., the Pareto front), and extracts from it the optimal solution (if any) that best satisfies all criteria [16]. The analysis technique was extensively tested using "synthetic data" from hydrodynamic simulations to extract gradients. The niched-Pareto GA was thereby shown to be an efficient algorithm to implement the self-consistent analysis of simultaneous x-ray space-integrated line spectra and monochromatic images and to uniquely determine core gradients.

The result of this analysis for the Δt_2 image and spectral data is illustrated in Figs. 2–4. Because of the 10 μm resolution in the data from each image, the spatial dependence of the gradients is characterized by values given in six spatial zones. The uncertainty in the gradient values (shaded area in Fig. 4) is related to the alternative gradients found in the vicinity of the optimal solution that produce comparable self-consistent fits using the range of input values produced by the deviation from spherical symmetry (see Fig. 3). In order to illustrate the accuracy of the fits, we also display in Figs. 2 and 3 the comparison between the data and the fits calculated with the self-consistent $T_e(r,t)$ and $N_e(r,t)$. Note that, for comparison with the image data, the streak spectrograph data must be integrated about the central time of the image over a time interval corresponding to the 40 ps frame time duration. Finally, as a check, the emissivity-weighted average values of the gradients shown in Fig. 4 are compared with the values of the electron temperature and density obtained from a fit to the He$_\beta$ lineout, presented in Fig. 2, using the same spectral model but assuming a uniform plasma core. These values, $\langle N_e \rangle = 3 \times 10^{23}$ cm^{-3} and $\langle T_e \rangle = 600$ eV, are consistent to within 4% with those obtained with a uniform plasma model analysis. This level of consistency, illustrated for

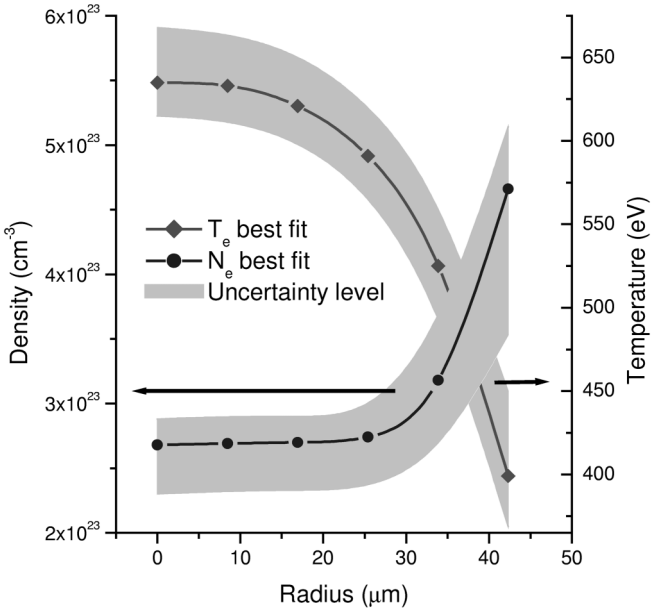

FIG. 4. Electron temperature and density profiles that yield the self-consistent fits shown in Figs. 2 and 3 for Δt_2. Estimates of the uncertainty in gradient values are indicated as the shaded area around the solid best fit curves.

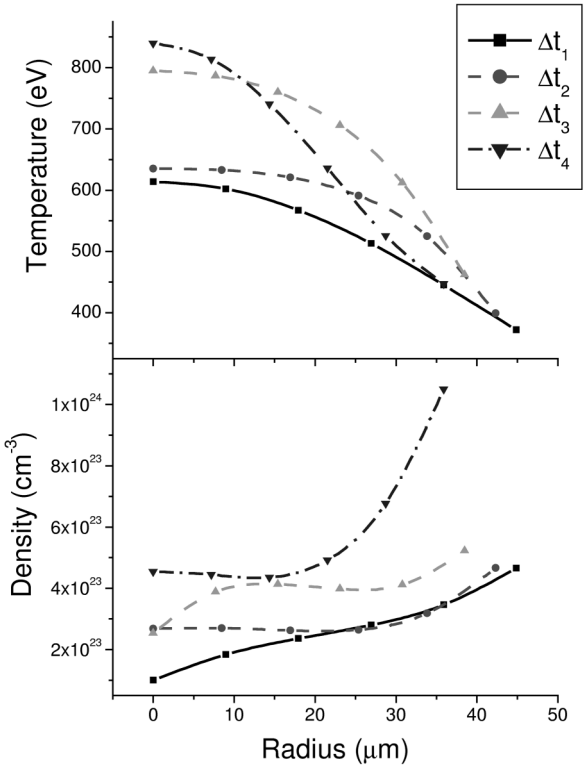

FIG. 5. Time-dependent sequence of the core plasma gradients of electron density, bottom graph, and temperature, top graph.

Δt_2, is typical of all the cases analyzed in this work. We note that, since the electron density N_e is largely a result of ionization of D atoms that are the dominant ion, the N_e gradient is also characteristic of the mass density gradient.

In conclusion, Fig. 5 shows the results from the analysis of four sequential time frames recorded by the monochromatic x-ray framing camera during the collapse of the implosion. Time Δt_2 is the same as in Figs. 1–4. Time Δt_4 corresponds to the peak of emission of the Heβ line. As a function of time, average electron temperature and density in the core increase. Densities close to the pusher boundary are larger than those at the center. Temperatures rise towards the center, and for the last time, Δt_4, a steeper gradient is observed. For later times, we see from the streak data that the space-integrated intensity of the Heβ line decreases quickly. In principle, this can be interpreted as the beginning of the core cool down. We note that temperature and density gradients obtained from this analysis are countercorrelated. This is consistent with an isobaric core at the collapse of the implosion, and it is also in qualitative agreement with results from 1D hydrodynamic code simulations. The uncertainties in the gradients result in considerable overlap of the four curves in Fig. 5, especially near the outer radius. However, it is important to note that the trend of the curves is clear and the overlap of individual curves does not detract from the analysis in spite of the uncertainties.

In this Letter, we present a unique determination of the dynamic temperature and density spatial gradients during the implosion phase of a laser compressed, high-energy-density plasma. The method is based on the self-consistent and simultaneous reconstruction and analysis of time-resolved x-ray line spectra and x-ray monochromatic images. We emphasize that the idea of using a niched-Pareto GA algorithm is general and can also be applied to other problems of multicriteria data analysis.

This work was supported in part by the DOE HEDS Grant No. DE-FG03-98DP00213 to Howard University. Support was also provided by LLNL under the auspices of DOE Contract No. W-7405-ENG-48, DOE NLUF Grant No. DE-FG03-01SF22225, NSF Grant No. 9624130, the ILS, the Japan-Germany and Japan-U.S. Collaboration Program of JSPS, and the Deutsche Forschungsgemeinschaft Contract No. FO186/3-1.

*Present address: Fusion Tech. Inst., University of Wisconsin, Madison, Wisconsin.

[1] B. Yaakobi *et al.,* Phys. Rev. Lett. **39**, 1526 (1977); K. B. Mitchell *et al.,* Phys. Rev. Lett. **42**, 232 (1979); J. D. Kilkenny *et al.,* Phys. Rev. A **22**, 2746 (1980); C. Keane *et al.,* Rev. Sci. Instrum. **61**, 2780 (1990).
[2] B. Hammel *et al.,* Phys. Rev. Lett. **70**, 1263 (1993); H. Nishimura *et al.,* Phys. Plasmas **2**, 2063 (1995); C. Hooper, Jr. *et al.,* Laser Part. Beams **14**, 713 (1996); D. Haynes, Jr. *et al.,* Phys. Rev. E **53**, 1042 (1996).
[3] N. Woolsey *et al.,* Phys. Rev. E **57**, 4650 (1998); N. Woolsey *et al.,* Phys. Rev. E **56**, 2314 (1997).
[4] Y. Ochi *et al.,* J. Quant. Spectrosc. Radiat. Transfer **65**, 393 (2000).
[5] N. Woolsey *et al.,* Phys. Rev. E **53**, 6396 (1996).
[6] H. Griem *et al.,* Phys. Fluids B **4**, 2346 (1992); L. Godbert *et al.,* Phys. Rev. E **49**, 5644 (1994).
[7] L. Godbert *et al.,* Phys. Rev. Lett. **81**, 5568 (1998).
[8] R. W. Lee, J. Quant. Spectrosc. Radiat. Transfer **2**, 87 (1982).
[9] B. Remington *et al.,* Phys. Plasmas **4**, 1994 (1997).
[10] I. Uschmann *et al.,* Appl. Opt. **39**, 5865 (2000).
[11] K. Mima *et al.,* Phys. Fluids **3**, 2077 (1996).
[12] I. Golovkin and R. Mancini, J. Quant. Spectrosc. Radiat. Transfer **65**, 273 (2000).
[13] B. Yaakobi *et al.,* Opt. Commun. **133**, 43 (1997).
[14] D. E. Goldberg, *Genetic Algorithms* (Addison-Wesley, Reading, MA, 1989).
[15] I. Golovkin *et al.,* J. Quant. Spectrosc. Radiat. Transfer (to be published).
[16] I. Golovkin *et al.,* in *Proceedings of the 2000 Congress on Evolutionary Computation* (IEEE, New York, 2000), p. 1521.